PRIMARY RESEARCH ARTICLE

Global Change Biology WILEY

Greening drylands despite warming consistent with carbon dioxide fertilization effect

Alemu Gonsamo[1] | Philippe Ciais[2] | Diego G. Miralles[3] | Stephen Sitch[4] | Wouter Dorigo[5] | Danica Lombardozzi[6] | Pierre Friedlingstein[7] | Julia E. M. S. Nabel[8] | Daniel S. Goll[9] | Michael O'Sullivan[4] | Almut Arneth[10] | Peter Anthoni[10] | Atul K. Jain[11] | Andy Wiltshire[12] | Philippe Peylin[2] | Alessandro Cescatti[13]

[1]School of Earth, Environment and Society, McMaster University, Hamilton, ON, Canada

[2]Laboratoire des Sciences du Climat et de l'Environnement, CEA CNRS UPSACLAY, Gif sur Yvette, France

[3]Hydro-Climate Extremes Lab (H-CEL), Ghent University, Ghent, Belgium

[4]College of Life and Environmental Sciences, University of Exeter, Exeter, UK

[5]Department of Geodesy and Geoinformation, Vienna University of Technology, Vienna, Austria

[6]National Center for Atmospheric Research (NCAR), Boulder, CO, USA

[7]College of Engineering, Mathematics and Physical Sciences, University of Exeter, Exeter, UK

[8]Max Planck Institute for Meteorology, Hamburg, Germany

[9]Department of Geography, University of Augsburg, Augsburg, Germany

[10]Institute of Meteorology and Climate Research, Karlsruhe Institute of Technology, Garmisch-Partenkirchen, Germany

[11]Department of Atmospheric Sciences, University of Illinois at Urbana-Champaign, Urbana, IL, USA

[12]Met Office Hadley Centre, Exeter, UK

[13]Joint Research Centre, European Commission, Ispra, Italy

Correspondence
Alemu Gonsamo, School of Earth, Environment and Society, McMaster University, Hamilton, ON, Canada.
Email: gonsamoa@mcmaster.ca

Funding information
Canada Research Chairs; Natural Sciences and Engineering Research Council of Canada, Grant/Award Number: DGECR-2020-00245 and RGPIN-2020-05708

Abstract

The rising atmospheric CO_2 concentration leads to a CO_2 fertilization effect on plants—that is, increased photosynthetic uptake of CO_2 by leaves and enhanced water-use efficiency (WUE). Yet, the resulting net impact of CO_2 fertilization on plant growth and soil moisture (SM) savings at large scale is poorly understood. Drylands provide a natural experimental setting to detect the CO_2 fertilization effect on plant growth since foliage amount, plant water-use and photosynthesis are all tightly coupled in water-limited ecosystems. A long-term change in the response of leaf area index (LAI, a measure of foliage amount) to changes in SM is likely to stem from changing water demand of primary productivity in water-limited ecosystems and is a proxy for changes in WUE. Using 34-year satellite observations of LAI and SM over tropical and subtropical drylands, we identify that a 1% increment in SM leads to 0.15% (±0.008, 95% confidence interval) and 0.51% (±0.01, 95% confidence interval) increments in LAI during 1982–1998 and 1999–2015, respectively. The increasing response of LAI to SM has contributed 7.2% (±3.0%, 95% confidence interval) to total dryland greening during 1999–2015 compared to 1982–1998. The increasing response of LAI to SM is consistent with the CO_2 fertilization effect on WUE in water-limited ecosystems, indicating that a given amount of SM has sustained greater amounts of photosynthetic

foliage over time. The LAI responses to changes in SM from seven dynamic global vegetation models are not always consistent with observations, highlighting the need for improved process knowledge of terrestrial ecosystem responses to rising atmospheric CO_2 concentration.

1 | INTRODUCTION

Primary productivity in terrestrial ecosystems is highly dependent on the atmospheric concentration of CO_2. As the CO_2 concentration rises, leaf-scale photosynthesis increases, which, in turn, can lead to additional growth and storage of organic matter in leaves, stems, roots and detritus (Prentice et al., 2001; Walker et al., 2021). In tandem, the amount of water needed to fix CO_2 during photosynthesis is reduced under rising atmospheric CO_2 concentration due to the partial closure of the stomata limiting plant transpiration (Field et al., 1995; Keenan et al., 2013). This means the effect of CO_2 fertilization on soil moisture (SM) savings is enhanced in areas where water availability limits photosynthesis because elevated CO_2 leads to enhanced plant water-use efficiency (WUE). Consequently, the soil water savings under elevated CO_2 in water-limited ecosystems can support more plant growth. Nonetheless, quantifying large-scale ecosystem responses to increasing atmospheric CO_2 based on sparse observations remains challenging due to complex non-linear interactions with climatic forcing and co-occurring nutrient limitations.

CO_2 fertilization effects have been studied in field experiments, dating back as early as the 1960s. These experiments provided strong physiological evidence that CO_2 enrichment increases plant growth on crop and horticultural plants under stable environmental conditions (Wittwer & Robb, 1964). The advent of free-air CO_2 enrichment facilities significantly expanded the application of manipulative experiments with elevated CO_2 to the ecosystem level, including treed ecosystems (Hendrey et al., 1999; Norby & Zak, 2011). However, the effect of elevated CO_2 on plant growth in treed ecosystems remains equivocal due to complex interactions with forest age, climate, nutrient limitation and respiratory processes. Efforts to study the magnitude of CO_2 fertilization using carbon cycle models remain challenging due to a lack of understanding of co-occurring nutrient limitations (Piao et al., 2013; Smith et al., 2016), among other uncertainties. An earlier global study attributed 40% of the satellite-observed greening trend for 1982–2006 to CO_2 fertilization (Los, 2013). A comparable study (Zhu et al., 2016) that incorporated factorial simulations of multiple global ecosystem models for 1982–2009 attributed 70% of the satellite-observed greening to CO_2 fertilization. Recent findings (Chen et al., 2019) suggest human land-use management as a dominant driver of Earth's greening. Previous satellite-based CO_2 fertilization assessments report a higher confidence in enhanced photosynthetic CO_2 uptake

and WUE concurrently with rising CO_2 concentration, and a lower confidence in our ability to directly attribute the relative changes in carbon uptake, WUE and biomass production to rising CO_2 concentration (Chen et al., 2019; Cheng et al., 2017; Donohue et al., 2013; Los, 2013; Smith et al., 2016, 2020; Zhu et al., 2016).

Satellite greenness records capture both structural (i.e., leaf area index, LAI) and biochemical (e.g., foliage chlorophyll content) attributes that can be used as indicators of plant cover and growth. Since vegetation density and soil water content are relatively low in drylands, satellite observations of both SM and vegetation activity have high retrieval accuracy (Gonsamo et al., 2019). The satellite observations show persistent greening of drylands since the 1980s (Figure 1). Higher LAI under elevated CO_2 implies an increase in primary productivity (McCarthy et al., 2006; Norby & Zak, 2011). An open-top chamber field experiment with elevated CO_2 combined with warming and drying, analogous to dryland ecosystems, revealed a tight coupling between LAI and SM (Dermody et al., 2007). In parallel, plant transpiration in dryland ecosystems is strictly water limited and therefore controlled by SM (Dermody et al., 2007; Seneviratne et al., 2010). From these considerations and due to the influence of CO_2 fertilization effect on WUE, an increase in magnitude of LAI response to changes in SM may be expected in drylands under elevated CO_2. In other words, an equivalent increment in SM may lead to a larger LAI increase under higher WUE due to decreasing transpiration per unit LAI with increasing CO_2 concentration. Drylands are dominated by responsive systems to CO_2 fertilization (Wullschleger et al., 2002) such as herbaceous plants, shrubs and small trees that largely rely on shallow zone SM and nutrients due to low rainfall intensity (Breman et al., 2001). Satellite observations of surface SM in drylands capture both instantaneous and antecedent precipitation inputs because large fraction of precipitation remains in the surface SM for many days (McColl et al., 2017).

To explore the effect of CO_2 fertilization on WUE, we quantify the response of LAI to interannual changes in SM (hereafter, $\delta LAI/\delta SM$) for 1982–2015 using growing-season satellite-based LAI (Zhu et al., 2013) and microwave multi-satellite surface SM (~2–5 cm depth) records (Dorigo et al., 2017). We also explore whether state-of-the art dynamic global vegetation models (DGVMs; Le Quéré et al., 2018) can capture the satellite observed changes in $\delta LAI/\delta SM$. Two types of DGVM simulations are used to isolate the impact of CO_2 fertilization on $\delta LAI/\delta SM$ from that of climate change, (1) simulation with varying atmospheric CO_2 and fixed climate forcing and (2) simulations with varying CO_2 and climate forcing. The study is limited
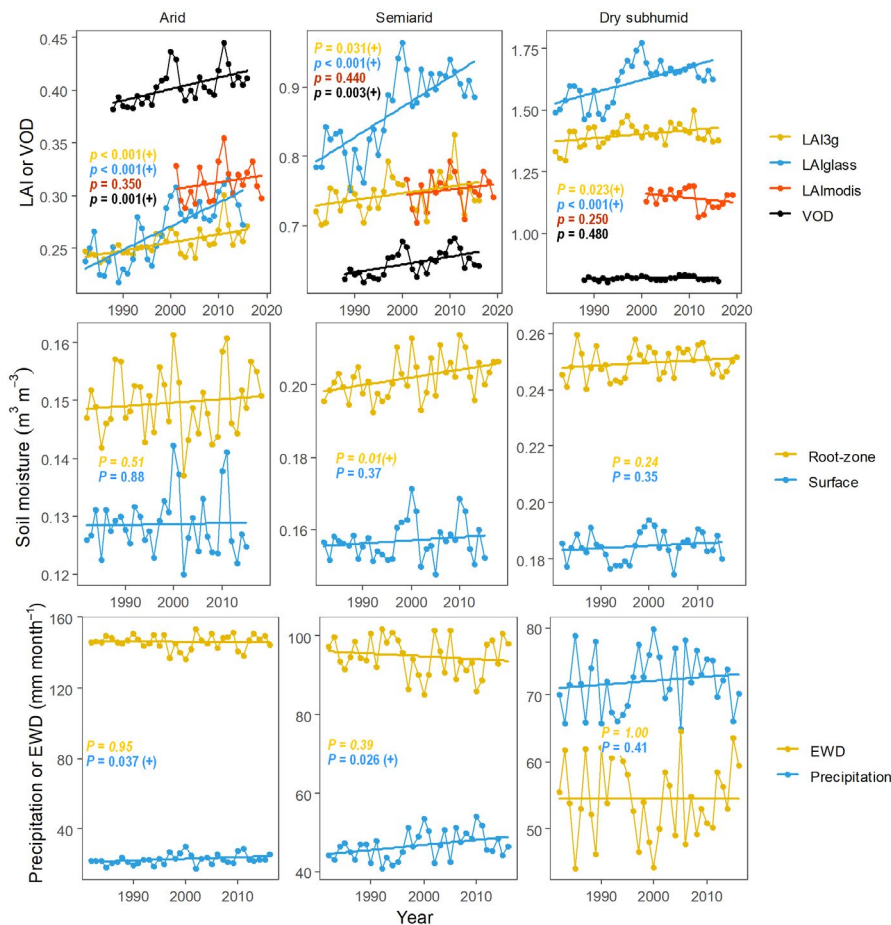
FIGURE 1 Trends in growing-season satellite leaf area index (LAI), vegetation optical depth (VOD), precipitation, ecosystem water demand (EWD) and soil moisture (SM) averaged at annual time scale for tropical and subtropical (35°S–35°N) drylands, that is, arid, semiarid and dry subhumid. Trend slope line and p value are presented in each panel while (+) and (−) indicating statistically significant ($p < 0.05$) increase and decrease, respectively, in the plotted variable. LAI time series from three data sources are plotted, namely, GIMMS LAI3g (Zhu et al., 2013) for 1982–2016, LAIglass (Xiao et al., 2014) for 1982–2015 and MODIS Terra Collection 6 LAI (LAImodis; Myneni et al., 2015) for 2001–2019. VOD time series is plotted for 1988–2016. VOD (Moesinger et al., 2020) is an independent measure of density, biomass and water content of vegetation derived from space-borne microwave radiometers that record radiation emitted by the Earth's surface at Ku-band. Surface SM from European Space Agency's Climate Change Initiative and root-zone SM from Global Land Evaporation Amsterdam Model (GLEAM) are derived from satellite observations. GLEAM root-zone SM is obtained by combining satellite surface SM with climate data and an empirical drainage model

to tropical and subtropical drylands (35°S–35°N) with the ratio of precipitation (P) to potential evapotranspiration (P/PET) of 0.05–0.65, excluding regions with more than 10% managed lands such as crop, urban and pasture lands derived from a 500 × 500 m resolution map. As declines in SM are often co-occurring with decreasing P, increasing air temperature, or increasing ecosystem water demand (EWD = PET-P, i.e., the balance between water inputs and potential evaporative demand) over time (Figure 1), direct climate impacts on LAI make the interpretation of changes in δLAI/δSM challenging. Therefore, we calculated δLAI/δSM as the partial derivative of LAI with respect to SM in a multiple regression of LAI against SM, temperature and EWD for earliest and recent 17-year periods of the satellite records, namely 1982–1998 and 1999–2015, and using different moving windows of 10, 15, and 20 years. The change in δLAI/δSM therefore directly reflects a change in LAI response to inter-annual changes in SM, rather than a potentially confounding direct

effect (not through SM) of temperature or EWD on LAI. The aim of our analysis is to determine temporal changes of δLAI/δSM during 1982–2015, and to relate observed changes to the CO_2 fertilization effect on WUE through deductive analysis of growing-season LAI, SM, P, temperature and EWD. We also test other potential hypotheses, including changes in climate and vegetation structure to explain the temporal changes in δLAI/δSM during the study period.

2 | MATERIALS AND METHODS

2.1 | Study area

Our analysis focuses on tropical and subtropical (35°S–35°N) drylands where a ratio of precipitation (P) to PET ranges between 0.05 and 0.65, which according to the UNEP definition include arid

(0.05–0.20 P/PET), semiarid (0.20–0.50 P/PET) and dry subhumid (0.50–0.65 P/PET) lands (Figure 2). Areas with more than 10% managed lands such as crop, urban and pasture lands were excluded based on the Moderate Resolution Imaging Spectroradiometer (MODIS) 500 m 2016 land-cover data (MCD12Q1, V6).

2.2 | Data

2.2.1 | Satellite LAI data

The global LAI data were obtained from the bi-weekly 8 km Global Inventory Modeling and Mapping Studies third-generation product (GIMMS LAI3 g) that are derived from surface reflectance observations from Advanced Very High-Resolution Radiometer (AVHRR; Zhu et al., 2013). LAI3g was generated using an artificial neural network trained on the Collection 6 Terra MODIS LAI product and the latest version (third generation) GIMMS AVHRR normalized difference vegetation index (NDVI) data for overlapping period. The GIMMS NDVI was carefully corrected for sensor degradation, intersensor differences, cloud cover, solar zenith angle, viewing angle effects due to satellite drift and volcanic aerosols (Zhu et al., 2013). LAI3g is proven to have an improved multi-sensor records harmonization scheme compared to other global LAI products (Forzieri et al., 2017). Nevertheless, we compare the LAI3g results with the 8-day 5 km Global LAnd Surface Satellite (GLASS) LAI (LAIglass) product, the latter compiled independently from AVHRR and MODIS satellite sensors (Xiao et al., 2014). Both satellite LAI products have been validated against field measurements over different biomes representative of global vegetated land covers (Xiao et al., 2014; Zhu et al., 2013). We restrict our analysis to 1982–2015 to coincide with the availability of reliable satellite LAI data. We compared trends in dryland LAI from LAI3 g and LAIglass with LAI derived from collection 6 MODIS Terra satellite (Myneni et al., 2015) and vegetation optical depth (VOD; Moesinger et al., 2020) derived from multiple satellite microwave radiometers (Figure 1). VOD (Moesinger et al., 2020) is an independent measure of density, biomass and water content of vegetation derived from space-borne microwave radiometers that record radiation emitted by the Earth's surface in Ku-band. Figure 1 shows the multiple lines of evidences for greening drylands.

2.2.2 | Satellite SM data

Daily SM data were obtained from the European Space Agency's Climate Change Initiative (ESA CCI) version 4.2 combined product, which is a merged passive and active microwave estimate of daily near-surface (~2–5 cm depth) SM content for 1982–2015 at 0.25° spatial resolution (Gruber et al., 2019). The retrieval rate and accuracy of CCI SM are high in drylands (Dorigo et al., 2017) while the data are either less reliable or not available in areas with high vegetation density, frozen soil, snow cover and glaciers. Validation of the earliest version CCI SM (version 0.1) against ground measurements resulted in root mean square error (RMSE) of <0.06 m^3 m^{-3} in semiarid areas in southeastern Australia (Albergel et al., 2013). To increase the robustness of our findings, we also obtained the root-zone SM data from Global Land Evaporation Amsterdam Model (GLEAM), version 3.3a at a spatial resolution of 0.25° for 1982–2018. The GLEAM SM is calculated by combining multi-source precipitation records, satellite-observed surface SM, VOD, snow-water equivalent and reanalysis air temperature and radiation with a simple empirical drainage algorithm to estimate surface and root-zone water content (Gonzalez Miralles et al., 2011; Martens et al., 2017). The GLEAM root-zone SM estimates were validated against 2325 global SM measurements across a broad range of ecosystems, resulting in normalized RMSE of <0.06 m^3 m^{-3} (Martens et al., 2017). Satellite observations of SM in drylands capture both instantaneous and antecedent precipitation inputs because a large fraction of precipitation remains in the surface SM for many days (McColl et al., 2017). Since vegetation density and soil water contents are low in drylands, both satellite-based SM and LAI estimates have high retrieval accuracy (Gonsamo et al., 2019).

2.2.3 | Gridded monthly land climate data

The monthly global minimum and maximum temperature, precipitation and PET data were obtained from the monthly gridded high-resolution TerraClimate archive (Abatzoglou et al., 2018) at 4 km × 4 km spatial resolution for 1982–2016. Monthly mean temperature is calculated by averaging the monthly minimum and maximum temperature. The high-resolution TerraClimate data are
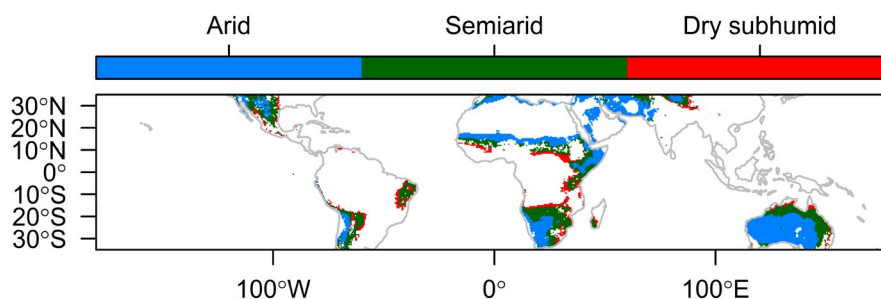

FIGURE 2 Spatial distribution of tropical and subtropical (35°S–35°N) drylands at 0.25° × 0.25° grid size excluding areas with more than 10% managed land. The dryland is separated into three zones following a ratio of precipitation (P) to potential evapotranspiration (PET) gradient to arid (0.05–0.20 P/PET), semiarid (0.20–0.50 P/PET) and dry subhumid (0.50–0.65 P/PET)

used along with the satellite observations of LAI and SM. To analyze the DGVM outputs, we obtained the monthly global temperature, precipitation and PET from the monthly gridded Climatic Research Unit (CRU TS 4.01; Harris et al., 2014) archive at $0.5° × 0.5°$ spatial resolution for 1901–2016. EWD, defining water relations between plants and climate as a balance between water input (precipitation) and potential output (energy, temperature), was calculated as PET minus precipitation. Large, positive EWD values indicate extremely dry while large negative values indicate extremely wet conditions.

2.2.4 | DGVM data

We obtained modeled fractional vegetation cover, SM and LAI from the DGVM outputs that participated in TRENDY v7 (trends in net land–atmosphere carbon exchanges) project (Le Quéré et al., 2018; Sitch et al., 2015). Data from the TRENDY project are a result of global modeling and synthesis efforts by a consortium of DGVM groups as a part of the Global Carbon Project. We excluded TRENDY models that do not provide monthly fractional vegetation cover, LAI and SM, the latter for each soil layer separately for 1901–2016. The selected seven TRENDY models include, CLM5.0 (Oleson et al., 2013), ISAM (Meiyappan et al., 2015), JSBACH (Mauritsen et al., 2019), JULES (Clark et al., 2011), LPJ-GUESS (Smith et al., 2014), ORCHIDEE (Krinner et al., 2005) and ORCHIDEE-CNP (Goll et al., 2017). For models that simulate the total LAI of each plant functional type (PFT), we sum LAI that belongs to natural vegetation in each grid cell. For models that provide fractional LAI per PFT, we extract a weighted LAI only from natural vegetation using the fractional vegetation cover provided with the model simulations. For LPJ-GUESS simulations, LAI of each year is obtained from the following year because of 1-year lag between the photosynthetically fixed carbon and the carbon allocated to the yearly photosynthetic leaf biomass in LPJ-GUESS simulations. The SM is extracted from the top layers that encompass the root-zone region ranging from 21.6 cm in ISAM to 50 cm in LPJ-GUESS (Table S1). JSBACH has a spatially explicit mean root-zone depth for each grid cell and simulates the SM for this root zone (Hagemann & Stacke, 2015) and therefore we use the simulated root-zone SM for JSBACH. All DGVMs that participated in TRENDY v7 project provide SM estimates in kg m^{-2}. We converted the DGVM root-zone SM estimate from kg m^{-2} to m^3 m^{-3} to make it consistent with the satellite observations of SM using the assumed rooting depth of each model, that is, the sum of the selected top soil layers depth or root-zone depth for JSBACH (Table S1) and assuming the density of water as 1 g cm^{-3}. The DGVMs have different spatial resolution, PFT definitions and C:N coupling mechanisms (Table S1). All DGVMs in the TRENDY project were driven with common forcing data including the CRU and Japanese Reanalysis climate data for simulations over the historical period (Le Quéré et al., 2018). We use two types of DGVM simulations: S1 that use varying atmospheric CO_2, fixed climate from 1901–1920, and fixed land use and land cover from 1860; and S2 that use varying CO_2 and climate with fixed land use and land cover from 1860. For each simulation, the DGVMs

first established an equilibrium state of carbon balance using a spin-up run, which is forced with the CO_2 concentration of the year 1700, recycling climate mean and variability from the early decades of the twentieth century (i.e., 1901–1920) and holding land-use constant.

2.3 | Methods

The bi-weekly LAI and daily SM data were averaged to monthly data using the values within each month. The LAI data are re-gridded to $0.25° × 0.25°$ equal area grids by taking the average of all LAI values within each grid to match with the spatial resolution of the SM data. All climate, SM and LAI data were aggregated to annual growing-season values using the mean values of the growing-season months to remove the impacts of seasonal changes on the LAI and SM relationship. The growing season for each grid cell was defined as months where monthly LAI values from the 34-year average climatology were greater than 0.2, meaning that the growing season varies spatially but is fixed across the years. Grid cells with less than 25 years of either SM or LAI data were removed from the analysis. A recent study suggested that woody vegetation foliage biomass increase in part of the Sahel is related to increased rains in early and late growing season (Brandt et al., 2019). To complement our analysis, we also extracted annually averaged early and late growing-season precipitation (ELP) from months with LAI values above 0.2 and below 50% of maximum monthly LAI. Therefore, ELP corresponds to the total precipitation that occurs before and after the core growing season.

The response of LAI to interannual changes in SM (δLAI/δSM, [m^2 m^{-2}]/[m^3 m^{-3}]) is calculated using annually averaged growing-season satellite-based LAI and microwave multi-satellite surface SM (~2–5 cm depth) records for 1982–2015 at annual time scale. δLAI/δSM is calculated as the partial derivative of LAI with respect to interannual changes in SM using a multiple regression of LAI against SM, temperature and EWD for earliest and recent 17-year periods, namely 1982–1998 and 1999–2015, and different moving windows of 10, 15 and 20 years for 1982–2015. Precipitation is excluded from the explanatory variables list after conducting variance inflation factor (VIF) analysis. Using the full 34-year data, we obtained mean VIF < 1.5 for SM, temperature and EWD indicating that there is no covariation among the selected three predictors at annual time scale. To complement our analysis, we also calculated δLAI/δSM and δLAI/δPre, where Pre stands for precipitation, using a simple linear regression of LAI against SM and LAI against precipitation, respectively. All datasets are detrended in each calculation window. The calculation of δLAI/δSM using a partial derivative in a multiple regression is well justified to capture possible emerging first-order temporal changes in long-term satellite observations (Forzieri et al., 2017, 2020). This approach factors out the direct effects of temperature and EWD on LAI that are not mediated by SM, and does not account for the possible covariation among predictors. To complement the analysis, we also calculated δLAI/δSM using two different satellite LAI data sources (i.e., LAI3g and LAIglass), and surface SM from ESA CCI and root-zone SM from GLEAM. To compare the

relative response of LAI to interannual changes in SM across different types of dryland zones, we calculated the percent response of LAI to SM (δLAI/δSM, %/%) by normalizing the 34-year record of LAI and SM values between 0% and 100% for each pixels:

$$Y_i(\%) = \frac{X_i - X_{min}}{X_{max} - X_{min}} \times 100, \quad (1)$$

where Y_i is the annual LAI or SM in %, X_i is the annual LAI or SM in native units, and X_{max} and X_{min} are the 34-year minimum and maximum LAI or SM in native units for each pixel, respectively.

We calculate the p value of SM slope in multiple regression conducted to obtain the partial derivative of LAI with respect to interannual changes in SM to test the null hypothesis that the SM slope is equal to zero (no effect) at pixel level. The pixel level p values are integrated into a single annual value for all study area or dryland zones following Fisher's method of combining independent tests. Since the spatial LAI and SM data are spatially autocorrelated, we select 500 random pixels to calculate Fisher's combined p value to keep the testing samples independent. We use the same procedure to calculate the combined p value for δLAI/δSM obtained from a simple linear regression.

In our analysis, the changes in δLAI/δSM directly reflect the changes in LAI response to interannual changes in SM, rather than a potentially confounding direct effect (not through SM) of climate on LAI. δLAI/δSM is an effective proxy of WUE in water-limited ecosystems of drylands for the following reasons: (1) Higher LAI under elevated CO_2 implies an increase in primary productivity (McCarthy et al., 2006; Norby & Zak, 2011). (2) An open-top chamber field experiment with elevated CO_2 combined with warming and drying, analogous to dryland ecosystems, indicated a tight coupling among LAI, plant water use and photosynthesis (Dermody et al., 2007). (3) Plant transpiration in dryland ecosystems is strictly water limited and therefore controlled by SM (Dermody et al., 2007; Seneviratne et al., 2010). The enhanced WUE as expressed in increasing δLAI/δSM is the result of reduced stomatal conductance and decreased transpiration per unit leaf area. In water-limited ecosystems, the increasing δLAI/δSM leads to soil water savings and consequent increase in plant-available soil water that can support more plant growth and greening. The contributions of changing LAI response to SM (δLAI^{SM}) to the long-term trend of LAI (δLAI) for recent (1999–2015) and earliest (1982–1998) 17-year periods are calculated based on the previously described approach (Forzieri et al., 2017, 2020) as follows:

$$\delta LAI^{SM}(\%) = \frac{\delta SM(\delta LAI/\delta SM)}{\delta LAI} \times 100, \quad (2)$$

where δSM and δLAI are the 17-year period trends of SM and LAI, respectively. In Equation (2), δLAI/δSM is quantified as partial derivative by factoring out potentially confounding direct effects of temperature and EWD. All variables are detrended for each period.

Since there can be multiple causes that can contribute to change in δLAI/δSM other than the CO_2 fertilization effect over the period 1982–2015, we test three mutually nonexclusive alternative hypotheses that may explain the changes in δLAI/δSM: (H1) long-term changes in climate; (H2) changes in rainfall seasonality (Brandt et al., 2019) and (H3) changes in vegetation demographics and structure. To test the three hypotheses, we analyze the difference of δLAI/δSM between 1999–2015 and 1982–1998 along climatic gradients for H2, along the ratio of ELP to total growing-season precipitation gradient for H3, and along tree cover change for H3. Tree cover change data are derived from daily AVHRR observations at 0.05° × 0.05° spatial resolution for 1982–2016 (Song et al., 2018).

We also calculate comparable δLAI/δSM response measure from DGVM outputs that participated in TRENDY v7 to assess whether or not changes in WUE of dryland greening from satellite observations are captured in model simulations. The seven DGVMs representing the TRENDY data have different grid sizes ranging from 0.5° × 0.5° to 2.0° × 2.0° (Table S1). Since all TRENDY DGVMs are forced by CRU and Japanese Reanalysis climate data, we use the CRU data to define the tropical dryland study area at each model grid size. First, we derive the ratio of precipitation to PET at original CRU grid size (i.e., 0.5° × 0.5°) using mean values obtained by averaging the entire 1901–2016 series. Then we re-grid the ratio to each TRENDY model grid size. Finally, the ratio of precipitation to PET ranging between 0.05 and 0.65 is used to define tropical and subtropical (35°S–35°N) drylands, the study area at each model grid size. We apply the same approach as the satellite observational data on TRENDY outputs to derive δLAI/δSM as a partial derivative of LAI with respect to interannual changes in SM in a multiple regression of LAI against SM, temperature and EWD for earliest and recent 58-year periods at the native grid resolutions of each model. δLAI/δSM is calculated for both S1 and S2 DGVM simulations to detangle the contributions of CO_2 fertilization and climate to changing δLAI/δSM. The growing-season P, temperature and EWD are obtained from the CRU data rather than the model outputs.

3 | RESULTS

3.1 | Satellite detection of changes in LAI response to SM during 1982–2015

δLAI/δSM significantly ($p < 0.05$) increased from 0.36 ± 0.02 to 1.33 ± 0.03 m^2 m^{-2}/m^3 m^{-3} in arid lands, from 0.59 ± 0.03 to 2.46 ± 0.05 m^2 m^{-2}/m^3 m^{-3} in semiarid lands and from 0.47 ± 0.05 to 2.40 ± 0.09 m^2 m^{-2}/m^3 m^{-3} in dry subhumid lands from 1982–1998 to 1999–2015 (Figure 3b; Table S2). This translates to, for 1% increase in SM, LAI increased from 0.23 ± 0.01% to 0.58 ± 001% in arid lands, from 0.10 ± 0.01% to 0.47 ± 001% in semiarid lands and from 0.06 ± 0.02% to 0.41±01% in dry subhumid lands from 1982–1998 to 1999–2015 (Figure 3c). The least proportional increase in δLAI/δSM occurred in dry subhumid lands, that is, LAI increased by 0.34 more percent points for 1% increase in SM during 1999–2015 compared to 1982–1998. Averaged for all

FIGURE 3 Changes in response of leaf area index (LAI) to soil moisture (SM) from satellite observations for arid, semiarid and dry subhumid drylands. $\delta LAI/\delta SM$ is the partial derivative of LAI with respect to SM in a multiple regression of LAI against SM and climate variables, and is calculated at the pixel level. (a) Spatial difference calculated as $\delta LAI/\delta SM$ of 1999–2015 minus $\delta LAI/\delta SM$ of 1982–1998 in LAI and SM units, $(m^2\ m^{-2})/(m^3\ m^{-3})$. $\delta LAI/\delta SM$ calculated for the earliest (1982–1998) and recent (1999–2015) 17-year period in LAI and SM units (i.e., $[m^2\ m^{-2}]/[m^3\ m^{-3}]$; b), and in relative LAI and SM units (i.e., $[\%/\%]$) in (c). The bars in (b) and (c) show the mean values of the entire spatial data and error bars are 95% confidence intervals of the mean
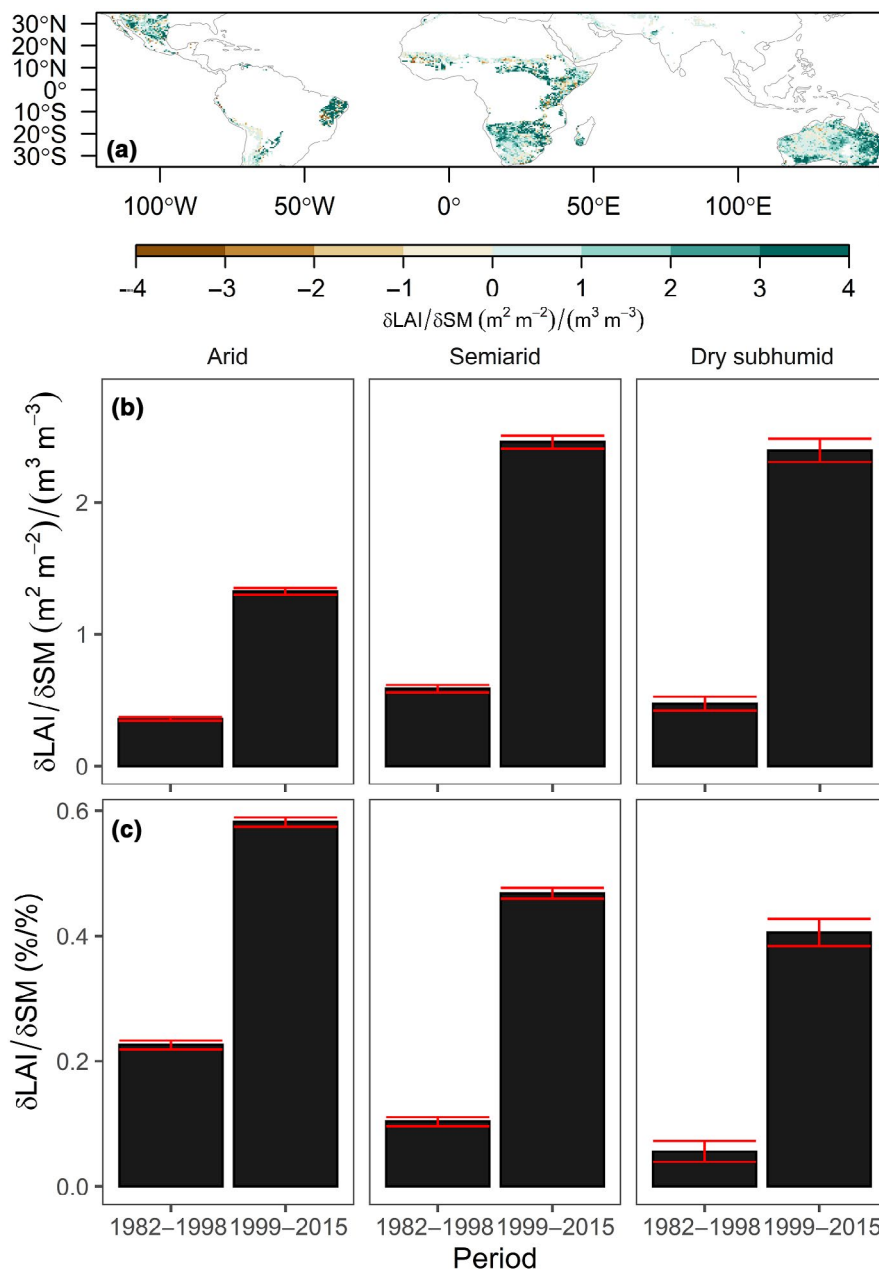
drylands, $\delta LAI/\delta SM$ increased from 0.47 ± 0.04 ($0.15 \pm 0.01\%/\%$) to $1.93 \pm 0.04\ m^2\ m^{-2}/m^3\ m^{-3}$ ($0.51 \pm 0.01\%/\%$) during 1999–2015 compared to 1982–1998.

The choice of the time period could affect the estimates of $\delta LAI/\delta SM$ changes; however, we found consistently increasing $\delta LAI/\delta SM$ since the 1980s from all three moving windows analyses (Figure 4). We also find a consistent increase in $\delta LAI/\delta SM$ since the 1980s from alternative satellite LAI (Figure S1), and from alternative satellite root-zone SM data (Figure S2), the latter obtained by combining the same satellite surface SM used in this study and climate data with a simple empirical drainage model to estimate root-zone water content (Martens et al., 2017). We find negative or close to zero $\delta LAI/\delta SM$ with low statistical significance in earlier periods of the satellite data records (Figure 4; Figure S1) with 10-year moving window analysis. To test whether or not this stems from artifacts in the multiple

regression model with low degree of freedom, we estimated $\delta LAI/\delta SM$ and $\delta LAI/\delta Pre$, where Pre is precipitation, using a simple linear regression and find consistently increasing $\delta LAI/\delta SM$ (Figure S3) and $\delta LAI/\delta Pre$ (Figure S4) since the 1980s. The slope of $\delta LAI/\delta SM$ (Figure S3) and $\delta LAI/\delta Pre$ (Figure S4) also remained significantly positive ($p < 0.05$) in simple linear regression.

The increasing $\delta LAI/\delta SM$ means a given amount of SM is progressively sustaining more foliage biomass over time, consistent with the CO_2 fertilization effect on plant growth, leading to the question of what role, if any, does the increasing $\delta LAI/\delta SM$ play in the long-term greening trends of drylands. We calculated the effects in greening that are strictly attributable to enhanced WUE by combining $\delta LAI/\delta SM$ estimate with the long-term trends of LAI and SM for the two 17-year periods independently. We found that the contribution of increasing $\delta LAI/\delta SM$ to the long-term greening increased from 6.5%
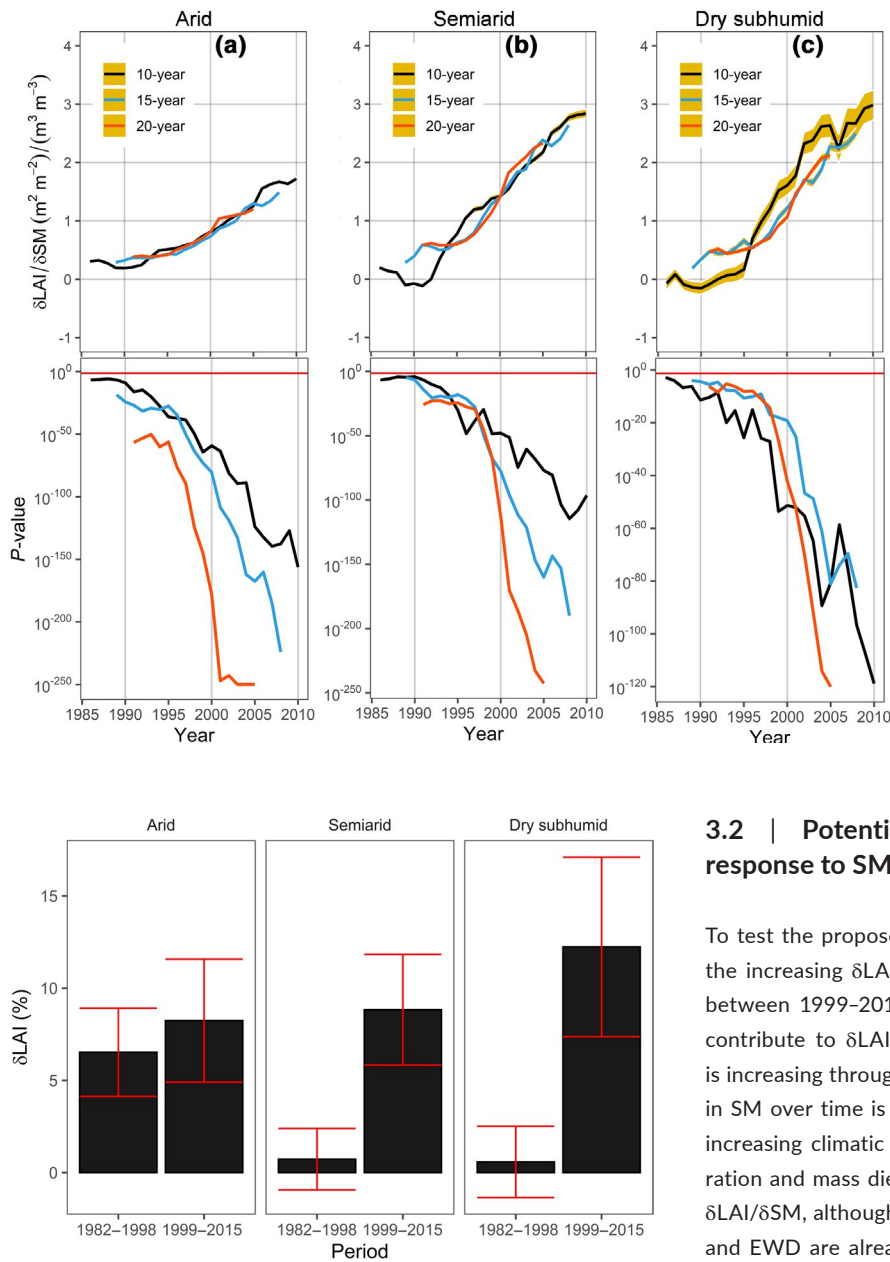
FIGURE 4 Changes in response of leaf area index (LAI) to soil moisture (SM) from satellite observations for arid (a), semiarid (b) and dry subhumid (c) drylands. The response of LAI to interannual changes in SM (i.e., δLAI/δSM) is calculated with 10-, 15- and 20-year moving windows. Years on the horizontal axis indicate the central year of the moving window. δLAI/δSM is the partial derivative of LAI with respect to SM in a multiple regression of LAI against SM and climate variables, and is calculated at the pixel level. The lines and shades in top panel show the mean values of the entire spatial data and 95% confidence intervals of the mean, respectively. Fisher's combined p values for the δLAI/δSM slope estimate are presented in bottom panels where a red horizontal line indicates $p = 0.05$

FIGURE 5 The contribution of enhanced water-use efficiency (WUE) to the long-term greening of drylands. The contribution of enhanced WUE to greening is calculated by multiplying the long-term trends of soil moisture (SM) with the response of leaf area index (LAI) to interannual changes in SM (δLAI/δSM) for recent (1999–2015) and earliest (1982–1998) 17-year periods. The resulting values are then divided by total LAI trends in each 17-year period to obtain the percent contributions. δLAI/δSM is quantified as partial derivative by factoring out potentially confounding direct effects of temperature and EWD. All datasets are detrended in each calculation window. All calculations are conducted at the pixel level. The bars show the mean values of the entire spatial data and the error bars are 95% confidence intervals of the mean

(±2.4%), 0.7% (±1.7%) and 0.6% (±1.9%) during 1982–1998 to 8.8% (±3.0%), 12.2% (±4.9%) and 11.2% (±4.9%) during 1999–2015 for arid, semiarid and dry subhumid drylands, respectively (Figure 5).

3.2 | Potential alternative causes of changes in LAI response to SM during 1982–2015

To test the proposed three potential hypotheses that may explain the increasing δLAI/δSM, we analyze the difference of δLAI/δSM between 1999–2015 and 1982–1998. First, climate warming may contribute to δLAI/δSM changes as growing-season temperature is increasing throughout the drylands (Figure S5). As severe decline in SM over time is often occurring with decreasing water input or increasing climatic water output, the long-term hydraulic deterioration and mass die-off of plants can also change the dynamics of δLAI/δSM, although the role of interannual changes in temperature and EWD are already accounted for in the δLAI/δSM calculation. We analyze the δLAI/δSM changes between the recent and earliest 17-year period across the 34-year climate trends, and find that the increase in δLAI/δSM occurred across all temperature, precipitation, EWD and SM trends (Figure 6). These results indicate that changes in long-term trends in precipitation and evapotranspiration have not contributed to the observed increases in δLAI/δSM.

Regarding the contribution of changes in rainfall seasonality to the increasing δLAI/δSM, the second hypothesis, recent findings (Brandt et al., 2019) suggested that on parts of the Sahel, areas with an increase in LAI of woody plants coincided with areas with increasing early and late growing-season precipitation (ELP). The argument is that annual herbaceous plants are vulnerable to dry spells, given their shallow rooting depth while woody plants are able to make use of sporadic ELP. In order to assess the contribution of increasing ELP to δLAI/δSM change, we extracted precipitation from months with LAI values between 0.2% and 50% of maximum LAI, corresponding to precipitation before and after the core growing season, or ELP.
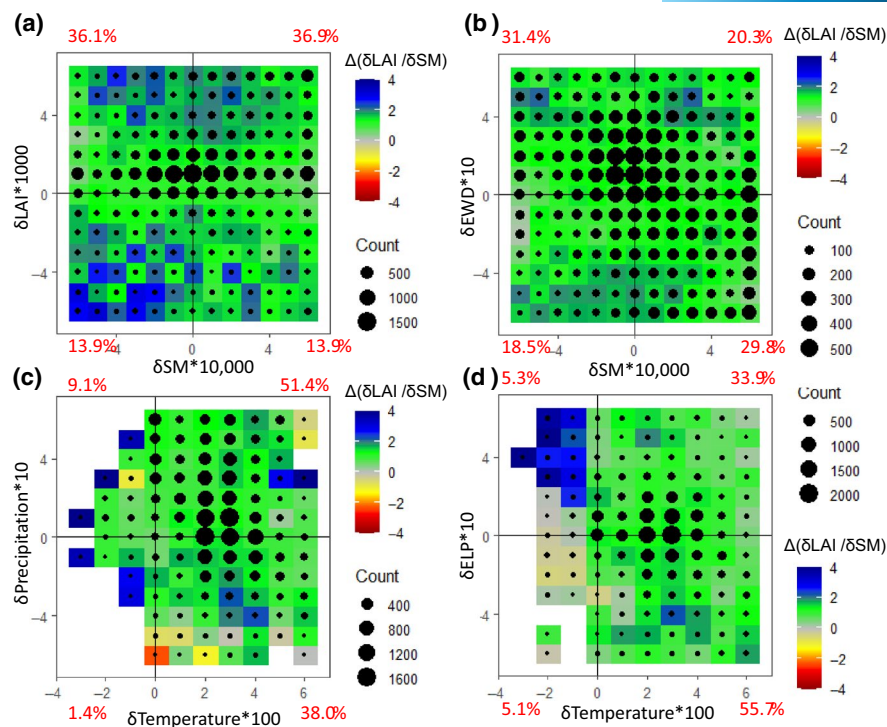
FIGURE 6 Changes in response of leaf area index (LAI) to soil moisture (SM) along long-term climate trends for drylands. Differences in response of LAI to interannual changes in SM (i.e., $\Delta[\delta LAI/\delta SM]$), calculated as $\delta LAI/\delta SM$ of 1999–2015 minus $\delta LAI/\delta SM$ of 1982–1998, plotted along the corresponding 34-year binned annual trend of SM (δSM, $m^3\ m^{-3}$) and LAI (δLAI, $m^2\ m^{-2}$; a), δSM ($m^3\ m^{-3}$) and ecosystem water demand (δEWD, mm month^{-1}; b), temperature ($\delta Temperature$, $^\circ C$) and precipitation ($\delta Precipitation$, mm month^{-1}; c), and temperature ($\delta Temperature$, $^\circ C$) and early and late season precipitation (δELP, mm year^{-1}; d). The count indicates the total number of dryland pixels in each binned category, and red labels indicate the percent fractions of the total dryland pixels that fall within each quadrant

We found a spatially sporadic increase in the ratio of ELP to total growing-season precipitation (Figure S6) consistent with the previous findings (Brandt et al., 2019) and inconsistent with the spatially widespread increase in $\delta LAI/\delta SM$ observed in drylands (Figure 3a). We also found no relationship between $\delta LAI/\delta SM$ difference between the two periods and the trend of the ratio of ELP to total growing-season precipitation (Figure S7). More than 50% of $\delta LAI/\delta SM$ increase in the recent period compared to the earliest 17-year period occurred where the ratio of ELP to total growing-season precipitation is decreasing (Figure 7d). Nonetheless, the increasing contribution of early and late season precipitation to the long-term increase in woody plant LAI does not necessarily preclude $\delta LAI/\delta SM$ increase.

Finally, the third attentive hypothesis for the possible causes of the increasing $\delta LAI/\delta SM$ in drylands are changes in vegetation demographics and structure, meaning changes in fraction of herbaceous and woody plants. These could be caused by woody plant encroachment, or changes in grazing, browsing and disturbances. Increased woody plant encroachment has been reported over semiarid areas during the satellite era (Brandt et al., 2019; Poulter et al., 2014). Using a high spatial resolution long-term percent tree cover change product (Song et al., 2018) in drylands, we found that the increase in $\delta LAI/\delta SM$ occurred both for increasing and decreasing tree cover areas (Figure S8). Changes in vegetation demographics and structure can also be caused by local-scale grazing, browsing and disturbances which are spatially inconsistent with widespread

increases in $\delta LAI/\delta SM$ observed throughout the tropical and subtropical drylands (Figure 3a).

3.3 | Changes in LAI response to SM during 1901–2016 in DGVMs

We used the output from seven DGVMs to test whether the observed CO_2 fertilization effect on WUE from satellite observations is captured in simulated LAI and root-zone SM in drylands. We only consider LAI of natural vegetation excluding crops and pastures from all seven DGVMs that simulate LAI and SM. Four models, namely ORCHIDEE, JSBACH, CLM5.0 and LPJ-GUESS show that CO_2 fertilization increases LAI response to interannual changes in SM both in earliest (1901–1958) and recent (1969–2016) CO_2 worlds (Figure 7), and for all three dry land types (Figure S9). Only LPJ-GUESS show statistically significant ($p < 0.05$) increase in $\delta LAI/\delta SM$ both from varying CO_2 alone, and varying CO_2 and climate simulations from 1901–1958 to 1959–2016 (Figure 8) consistent with the satellite observations. However, this increase from LPJ-GUESS is only observed in arid and semiarid drylands not in dry subhumid zones (Figures S10 and S11). CLM5.0 also shows statistically significant ($p < 0.05$) increase in $\delta LAI/\delta SM$ from varying CO_2 alone simulation from 1901–1958 to 1959–2016 (Figure 8; Table S3).

All seven models show greening drylands with increasing LAI (Figure S12) both from varying CO_2 alone, and varying CO_2 and
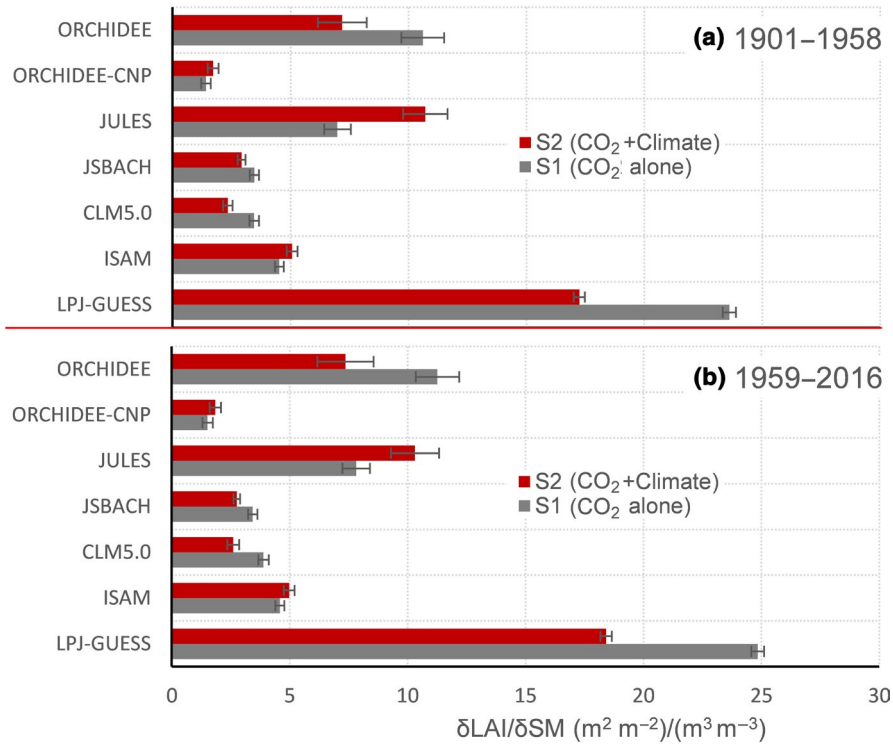
FIGURE 7 Changes in response of leaf area index (LAI) to soil moisture (SM) from seven dynamic global vegetation models for drylands. The response of LAI to interannual changes in root-zone SM (i.e., $\delta LAI/\delta SM$ [m^2 m^{-2}]/[m^3 m^{-3}]) is plotted for S2 simulations that are forced with changing CO_2 and climate (S2 CO_2+Climate), and S1 simulations that are forced with changing CO_2 alone (S1 CO_2 alone) during earliest (1901–1958) in (a), and recent (1959–2016) in (b) 58-year periods. $\delta LAI/\delta SM$ from models is estimated using root-zone SM with varying soil depth (Table S1). $\delta LAI/\delta SM$ is the partial derivative of LAI with respect to SM in a multiple regression of LAI against SM and climate variables, and is calculated at the pixel level. The bars show the mean values of the entire spatial data and error bars are 95% confidence intervals of the mean
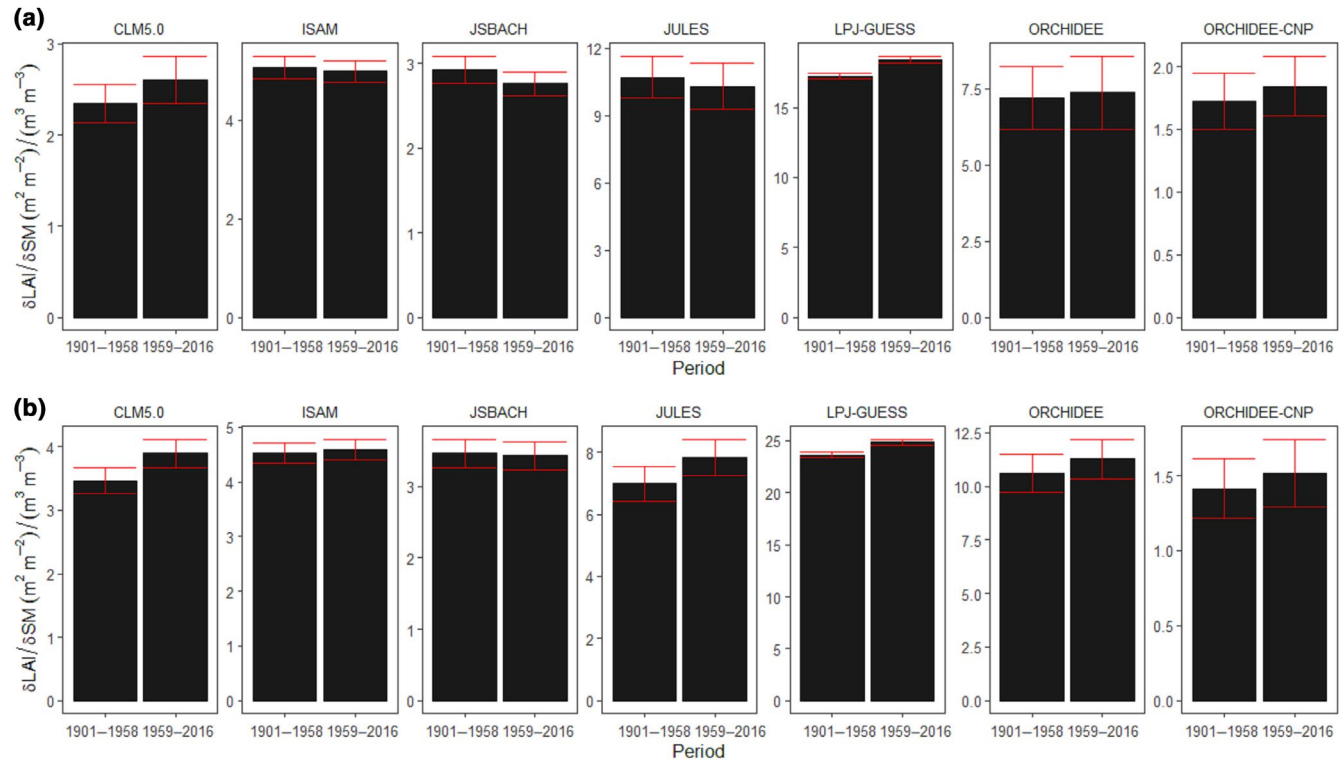
FIGURE 8 Changes in response of leaf area index (LAI) to soil moisture (SM) from seven dynamic global vegetation models for drylands. The response of LAI to interannual changes in root-zone SM (i.e., $\delta LAI/\delta SM$ [m^2 m^{-2}]/[m^3 m^{-3}]) for earliest (1901–1958) and recent (1959–2016) 58-year periods are plotted for S2 simulations that are forced with changing CO_2 and climate in (a), and S1 simulations that are forced with changing CO_2 alone in (b). $\delta LAI/\delta SM$ from models is estimated using root-zone SM with varying soil depth (Table S1). $\delta LAI/\delta SM$ is the partial derivative of LAI with respect to SM in a multiple regression of LAI against SM and climate variables, and is calculated at the pixel level. The bars show the mean values of the entire spatial data and error bars are 95% confidence intervals of the mean

climate simulations consistent with the satellite observations. Five out of the seven models, namely CLM5.0, ISAM, LPJ-GUESS, ORCHIDEE and ORCHIDEE-CNP show no change in long-term trend of SM (Figure S12) both from varying CO_2 alone, and varying CO_2 and climate simulations consistent with the satellite surface and root-zone SM observations. All models, except ISAM show strong positive correlation between simulated SM and LAI for both varying CO_2 alone, and varying CO_2 and climate simulations (Figure S13). The discrepancy of $\delta LAI/\delta SM$ changes between the satellite observations and DGVMs can be related to how well do DGVMs simulate SM and LAI. We found a strong significant interannual correlation ($p < 0.05$) between satellite-observed root-zone SM and simulated root-zone SM from varying CO_2 and climate simulations, comparable simulation to satellite observations, from all DGVMs (Figure S14a). However, LAI from DGVMs shows on average positive but statistically weak interannual relationship with satellite observations (Figure S14b).

4 | DISCUSSION

Multiple independent satellite data records and DGVM outputs all show greening drylands in the absence of changes in SM or significant shifts in precipitation and ecosystem water input and output regimes (Figure 1; Figure S12). Satellite data records indicated an overall increase in photosynthetic foliage biomass that can be sustained per unit volume of soil water content over time. As analyzed through $\delta LAI/\delta SM$, the proportional response of LAI to unit changes in SM generally increases with increasing aridity both in earlier and recent 17-year periods. This is expected as drier ecosystems are more sensitive to changes in SM than wetter ecosystems. This result suggest that $\delta LAI/\delta SM$ is a valid metric for water–plant relationship assessment in water-limited ecosystems under different CO_2 world. Although no difference is detected in proportional change of $\delta LAI/\delta SM$ from 1982–2015 to 1982–2015 between arid and semiarid ecosystems, the proportional increase in $\delta LAI/\delta SM$ was larger in both ecosystems than in dry sub-humid ecosystems (Figure 3). This is in line with the enhanced effect of CO_2 fertilization expected in areas where water availability limits photosynthesis because elevated CO_2 leads to enhanced WUE and soil water saving that can support more plant growth. EWD is at least twice the precipitation input during the growing season for both arid and semiarid drylands (Figure 1). Therefore, these ecosystems are always water limited and the proportional change in $\delta LAI/\delta SM$ between the recent and earlier period should be similar in both ecosystems.

Since there can be multiple causes that can contribute to $\delta LAI/\delta SM$ change other than the CO_2 fertilization effect over the period 1982–2015, we tested three alternative hypotheses, namely, (H1) long-term changes in climate; (H2) changes in rainfall seasonality and (H3) changes in vegetation demographics and structure, and found that none of them explain the observed increase in $\delta LAI/\delta SM$. To attribute the increasing $\delta LAI/\delta SM$ to the CO_2 fertilization effect, we use $\delta LAI/\delta SM$ calculated using a simple and multiple regressions with various sources of LAI and ecosystem water status, and relate the observed changes to the CO_2 fertilization effect on WUE through deductive analysis of the growing-season LAI, SM, P, temperature and EWD. Our results support the hypothesis that a given amount of SM sustains greater amounts of photosynthetic foliage over time in water-limited ecosystems in response to increasing atmospheric CO_2 centration, consistent with the theoretical expectations and field experiments. Greening associated with the CO_2 fertilization effect on photosynthetic uptake of CO_2 increases the amount of transpiring leaf area, and in principle total plant water consumption (Cheng et al., 2017; Ukkola et al., 2016); as a result, $\delta LAI/\delta SM$ may decline or become negative over time. However, if accompanied by an increase in WUE, the CO_2 fertilization effect may result in reduced stomatal conductance (Norby & Zak, 2011; Wullschleger et al., 2002) and decreased transpiration per unit leaf area; as a result, $\delta LAI/\delta SM$ may progressively increase in water-limited ecosystems. Therefore, our findings suggest that the dominant CO_2 fertilization effect in drylands is the enhanced WUE, consistent with experimental findings. Plot and field experiments with elevated CO_2 in dry environments indicated that the CO_2 fertilization effect on WUE is mediated through changes in LAI and SM (Dermody et al., 2007; Wullschleger et al., 2002). These studies showed increasing LAI under elevated CO_2 for stands with lower LAI ($<3.5\ m^2\ m^{-2}$; Norby & Zak, 2011), grasslands (Wullschleger et al., 2002), and warmer and drier fields (Dermody et al., 2007), all typical of dryland ecosystems and consistent with our results that show increasing LAI over drylands from multiple satellite sensors (Figure 1). The elevated CO_2 experiments in water-limited ecosystems (Wullschleger et al., 2002), satellite data records (Figure 1) and DGVM model outputs (Figure S12) all show negligible changes in SM despite increasing LAI, implying that the soil water savings from the enhanced WUE in water-limited ecosystems are spent to support more greening. This is supported by recent findings from field experiment in xeric and mesic habitat species in Australia where elevated atmospheric CO_2 is shown to benefit plants during drought by reducing stomatal conductance but the water savings are compensated by concurrent increase in leaf area (Jiang et al., 2021).

Our analysis provides observational evidence for increasing response of foliage biomass to interannual changes in SM in drylands since the 1980s. Although the observed increase in LAI response to SM is in expected direction of the CO_2 fertilization effect on WUE, the change in magnitude between the earliest and recent period is larger than expected. Several factors may contribute to the observed large increase besides the short time period of the satellite data record. The LAI time series are based upon multiple sensor systems as such the sensor shifts potentially can introduce uncertainties and artifacts in the analysis. The moving window analysis and detrending the dataset in each successive window can partially compensate errors related to sensor shifts. However, errors related to sensor shifts can still contribute to the observed large increase in LAI response to SM if sensors used for recent years are detecting LAI in areas with low vegetation cover better than older sensors due to the progressively improving radiometric performances of newer sensors. It is likely that the progressively improving spectral configurations and radiometric performance of the LAI and SM sensors may strengthen the covariation between the two variables that can

amplify the observed changes in LAI response to SM. Nonetheless, the observed increases in LAI responses to root-zone SM and precipitation are relatively smaller than the increase in LAI response to surface SM (Figure S4; Table S2).

The observed increase in LAI response to SM is not directly attributable to trends in specific climate variables or vegetation structural changes, and is consistent with the CO_2 fertilization effect on WUE. The increase in WUE with rising atmospheric CO_2 has long been postulated to lead to increased leaf area in global drylands (Farquhar, 1997). We identify that an equivalent increment in SM leads to a larger increase in LAI and has contributed 7.2% (±3.0%) to total dryland greening during 1999–2015 compared to 1982–1998. The remaining dryland greening observed from satellite data could arise from increased woody plant encroachment (Brandt et al., 2019; Poulter et al., 2014; Stevens et al., 2017; Tian et al., 2017; Venter et al., 2018), changes in rainfall distribution (Brandt et al., 2019; Gherardi & Sala, 2015; Kulmatiski & Beard, 2013), to mention but a few. Overall, our results indicate that the direct biochemical impact of the rapid increase in atmospheric CO_2 on terrestrial vegetation is detectable from satellites and should be considered as an important land surface process in future improvements of DGVMs and Earth System Models. Our results further suggest that the increasing WUE from CO_2 fertilization is compensated by increased water consumption, and less likely mitigates soil water scarcity in arid regions.

One limitation of our analysis is the root-zone SM relevant to deep-rooted plants is not directly measurable by satellites. This concern is compensated by consistent findings of $\delta LAI/\delta SM$ changes both from satellite observed surface SM, and root-zone SM, the latter estimated by combining the same satellite surface SM and climate data with a simple empirical drainage model. The LAI response to interannual changes in precipitation, the latter calculated solely from climate variables, shows increasing response of dryland greening to precipitation input over time as expected from CO_2 fertilization effect on WUE in water-limited ecosystems. These results indicate that the uncertainty in SM observations has not contributed to the observed changes in $\delta LAI/\delta SM$. Among the seven DGVMs analyzed in this study, only one model, namely JSBACH, has a spatially explicit mean root-zone depth for each grid cell and simulates the SM for this root zone (Hagemann & Stacke, 2015). Hence, some uncertainties exist in SM estimates both from satellite observations and DGVMs. Nonetheless, DGVM-simulated SM shows strong positive correlation with satellite observed root-zone SM, indicating uncertainties in SM simulations may have contributed negligibly to the observed discrepancy between the satellite and DGVM LAI responses to SM. Earlier analysis of the DGVMs used in this study suggested that increasing gross primary productivity simulated by the models over time in response to CO_2 fertilization is responsible for the increasing LAI (Zhu et al., 2016). However, the simulated LAI in our study shows poor relationship with observations indicating the discrepancy of LAI response to SM between the satellite observations and DGVMs could largely be linked to uncertainties in LAI simulations. Representation of C_3 and C_4 plants which respond differently to CO_2 fertilization, and the allocation and timing of photosynthetically fixed carbon to foliage biomass, varies among DGVMs may contribute to the observed discrepancy of LAI response to SM. While we are confident of the conclusion of our findings in water-limited ecosystems since satellite-based LAI and SM observations are of high quality in drylands, future improvements in simulations of LAI and SM will allow disentangling the distinct effect of CO_2 fertilization on photosynthetic uptake of CO_2 by plant leaves and WUE.

CONFLICT OF INTEREST

We declare we have no competing interests.

AUTHOR CONTRIBUTION

Alemu Gonsamo conceived the general idea and designed the study with the contribution from Alessandro Cescatti, Philippe Ciais, Diego G. Miralles, Stephen Sitch, Pierre Friedlingstein and Michael O'Sullivan. Danica Lombardozzi, Julia E. M. S. Nabel, Daniel S. Goll, Almut Arneth, Peter Anthoni, Atul K. Jain, Andy Wiltshire and Philippe Peylin provided DGVM outputs. Alemu Gonsamo wrote the initial draft and all co-authors contributed to editing the manuscript and gave final approval for publication.

DATA AVAILABILITY STATEMENT

The latest GIMMS LAI3g data are available at Baidu Netdisk (http://pan.baidu.com/s/1mhK2zTA) and Google Drive (https://drive.google.com/open?id=0BwL88nwumpqYaFJmR2poS0d1ZDQ https://ecocast.arc.nasa.gov/data/pub/gimms/). The GLASS leaf area index is available at http://www.glass.umd.edu/Download.html. The CCI soil moisture is available at https://www.esa-soilmoisture-cci.org/node/145. The GLEAM soil moisture is available at https://www.gleam.eu/. The vegetation optical depth data are available at https://zenodo.org/record/2575599#.X4DKJGhKhnI. The MODIS satellite observations are available at https://search.earthdata.nasa.gov/search. The TerraClimate data are available at https://climatedataguide.ucar.edu/climate-data/terraclimate-global-high-resolution-gridded-temperature-precipitation-and-other-water. The CRU climate data are available at https://crudata.uea.ac.uk/cru/data/hrg/. Simulations from seven DGVMs (LPJ-GUESS, ISAM, CLM5.0, JSBACH, JULES, ORCHIDEE-CNP and ORCHIDEE) are available from the TRENDY dataset on request from S.S. All generated data and R code used to process and analyze the data are available from the corresponding author on request.

ORCID

Alemu Gonsamo https://orcid.org/0000-0002-2461-618X
Danica Lombardozzi https://orcid.org/0000-0003-3557-7929
Michael O'Sullivan https://orcid.org/0000-0002-6278-3392
Atul K. Jain https://orcid.org/0000-0002-4051-3228

REFERENCES

Abatzoglou, J. T., Dobrowski, S. Z., Parks, S. A., & Hegewisch, K. C. (2018). TerraClimate, a high-resolution global dataset of monthly climate and climatic water balance from 1958–2015. *Scientific Data*, 5(1), 1–12. https://doi.org/10.1038/sdata.2017.191

Albergel, C., Dorigo, W., Reichle, R. H., Balsamo, G., de Rosnay, P., Muñoz-Sabater, J., Isaksen, L., de Jeu, R., & Wagner, W. (2013). Skill and global trend analysis of soil moisture from reanalyses and microwave remote sensing. *Journal of Hydrometeorology*, 14(4), 1259–1277. https://doi.org/10.1175/JHM-D-12-0161.1

Brandt, M., Hiernaux, P., Rasmussen, K., Tucker, C. J., Wigneron, J.-P., Diouf, A. A., Herrmann, S. M., Zhang, W., Kergoat, L., Mbow, C., Abel, C., Auda, Y., & Fensholt, R. (2019). Changes in rainfall distribution promote woody foliage production in the Sahel. *Communications Biology*, 2(1), 1–10. https://doi.org/10.1038/s42003-019-0383-9

Breman, H., Groot, J. R., & van Keulen, H. (2001). Resource limitations in Sahelian agriculture. *Global Environmental Change*, 11(1), 59–68. https://doi.org/10.1016/S0959-3780(00)00045-5

Chen, C., Park, T., Wang, X., Piao, S., Xu, B., Chaturvedi, R. K., Fuchs, R., Brovkin, V., Ciais, P., Fensholt, R., Tømmervik, H., Bala, G., Zhu, Z., Nemani, R. R., & Myneni, R. B. (2019). China and India lead in greening of the world through land-use management. *Nature Sustainability*, 2(2), 122–129. https://doi.org/10.1038/s41893-019-0220-7

Cheng, L., Zhang, L. U., Wang, Y.-P., Canadell, J. G., Chiew, F. H. S., Beringer, J., Li, L., Miralles, D. G., Piao, S., & Zhang, Y. (2017). Recent increases in terrestrial carbon uptake at little cost to the water cycle. *Nature Communications*, 8(1), 110. https://doi.org/10.1038/s41467-017-00114-5

Clark, D. B., Mercado, L. M., Sitch, S., Jones, C. D., Gedney, N., Best, M. J., Pryor, M., Rooney, G. G., Essery, R. L. H., Blyth, E., Boucher, O., Harding, R. J., Huntingford, C., & Cox, P. M. (2011). The Joint UK Land Environment Simulator (JULES), model description – Part 2: Carbon fluxes and vegetation dynamics. *Geoscientific Model Development*, 4(3), 701–722. https://doi.org/10.5194/gmd-4-701-2011

Dermody, O., Weltzin, J. F., Engel, E. C., Allen, P., & Norby, R. J. (2007). How do elevated [CO_2], warming, and reduced precipitation interact to affect soil moisture and LAI in an old field ecosystem? *Plant and Soil*, 301(1), 255–266. https://doi.org/10.1007/s11104-007-9443-x

Donohue, R. J., Roderick, M. L., McVicar, T. R., & Farquhar, G. D. (2013). Impact of CO_2 fertilization on maximum foliage cover across the globe's warm, arid environments. *Geophysical Research Letters*, 40(12), 3031–3035. https://doi.org/10.1002/grl.50563

Dorigo, W., Wagner, W., Albergel, C., Albrecht, F., Balsamo, G., Brocca, L., Chung, D., Ertl, M., Forkel, M., Gruber, A., Haas, E., Hamer, P. D., Hirschi, M., Ikonen, J., de Jeu, R., Kidd, R., Lahoz, W., Liu, Y. Y., Miralles, D., … Lecomte, P. (2017). ESA CCI soil moisture for improved Earth system understanding: State-of-the art and future directions. *Remote Sensing of Environment*, 203, 185–215. https://doi.org/10.1016/j.rse.2017.07.001

Farquhar, G. D. (1997). Carbon dioxide and vegetation. *Science*, 278(5342), 1411. https://doi.org/10.1126/science.278.5342.1411

Field, C. B., Jackson, R. B., & Mooney, H. A. (1995). Stomatal responses to increased CO_2: Implications from the plant to the global scale. *Plant, Cell and Environment*, 18(10), 1214–1225. https://doi.org/10.1111/j.1365-3040.1995.tb00630.x

Forzieri, G., Alkama, R., Miralles, D. G., & Cescatti, A. (2017). Satellites reveal contrasting responses of regional climate to the widespread greening of Earth. *Science*, 356(6343), 1180–1184. https://doi.org/10.1126/science.aal1727

Forzieri, G., Miralles, D. G., Ciais, P., Alkama, R., Ryu, Y., Duveiller, G., Zhang, K. E., Robertson, E., Kautz, M., Martens, B., Jiang, C., Arneth, A., Georgievski, G., Li, W., Ceccherini, G., Anthoni, P., Lawrence, P., Wiltshire, A., Pongratz, J., … Cescatti, A. (2020). Increased control of vegetation on global terrestrial energy fluxes.

Nature Climate Change, 10(4), 356–362. https://doi.org/10.1038/s41558-020-0717-0

Gherardi, L. A., & Sala, O. E. (2015). Enhanced precipitation variability decreases grass-and increases shrub-productivity. *Proceedings of the National Academy of Sciences of the United States of America*, 112(41), 12735–12740. https://doi.org/10.1073/pnas.1506433112

Goll, D., Vuichard, N., Maignan, F., Jornet-Puig, A., Sardans, J., Violette, A., & Guimberteau, M. (2017). A representation of the phosphorus cycle for ORCHIDEE (revision 4520). *Geoscientific Model Development*, 10(10), 3745–3770. https://doi.org/10.5194/gmd-10-3745-2017

Gonsamo, A., Chen, J. M., He, L., Sun, Y., Rogers, C., & Liu, J. (2019). Exploring SMAP and OCO-2 observations to monitor soil moisture control on photosynthetic activity of global drylands and croplands. *Remote Sensing of Environment*, 232, 111314. https://doi.org/10.1016/j.rse.2019.111314

Gonzalez Miralles, D., Holmes, T., De Jeu, R., Gash, J., Meesters, A., & Dolman, A. (2011). Global land-surface evaporation estimated from satellite-based observations. *Hydrology and Earth System Sciences*, 15(2), 453–469. https://doi.org/10.5194/hess-15-453-2011

Gruber, A., Scanlon, T., van der Schalie, R., Wagner, W., & Dorigo, W. (2019). Evolution of the ESA CCI soil moisture climate data records and their underlying merging methodology. *Earth System Science Data*, 11(2), 717–739. https://doi.org/10.5194/essd-11-717-2019

Hagemann, S., & Stacke, T. (2015). Impact of the soil hydrology scheme on simulated soil moisture memory. *Climate Dynamics*, 44(7), 1731–1750. https://doi.org/10.1007/s00382-014-2221-6

Harris, I., Jones, P. D., Osborn, T. J., & Lister, D. H. (2014). Updated high-resolution grids of monthly climatic observations – The CRU TS3.10 Dataset. *International Journal of Climatology*, 34(3), 623–642. https://doi.org/10.1002/joc.3711

Hendrey, G. R., Ellsworth, D. S., Lewin, K. F., & Nagy, J. (1999). A free-air enrichment system for exposing tall forest vegetation to elevated atmospheric CO_2. *Global Change Biology*, 5(3), 293–309. https://doi.org/10.1046/j.1365-2486.1999.00228.x

Jiang, M., Kelly, J. W., Atwell, B. J., Tissue, D. T., & Medlyn, B. E. (2021). Drought by CO_2 interactions in trees: A test of the water savings mechanism. *New Phytologist*, 230, 1421–1434. https://doi.org/10.1111/nph.17233

Keenan, T. F., Hollinger, D. Y., Bohrer, G., Dragoni, D., Munger, J. W., Schmid, H. P., & Richardson, A. D. (2013). Increase in forest water-use efficiency as atmospheric carbon dioxide concentrations rise. *Nature*, 499(7458), 324–327. https://doi.org/10.1038/nature12291

Krinner, G., Viovy, N., de Noblet-Ducoudré, N., Ogée, J., Polcher, J., Friedlingstein, P., Ciais, P., Sitch, S., & Prentice, I. C. (2005). A dynamic global vegetation model for studies of the coupled atmosphere-biosphere system. *Global Biogeochemical Cycles*, 19(1), GB1015. https://doi.org/10.1029/2003GB002199

Kulmatiski, A., & Beard, K. H. (2013). Woody plant encroachment facilitated by increased precipitation intensity. *Nature Climate Change*, 3(9), 833–837. https://doi.org/10.1038/nclimate1904

Le Quéré, C., Andrew, R. M., Friedlingstein, P., Sitch, S., Hauck, J., Pongratz, J., Pickers, P. A., Korsbakken, J. I., Peters, G. P., Canadell, J. G., Arneth, A., Arora, V. K., Barbero, L., Bastos, A., Bopp, L., Chevallier, F., Chini, L. P., Ciais, P., Doney, S. C., … Zheng, B. O. (2018). Global carbon budget 2018. *Earth System Science Data*, 10(4), 2141–2194. https://doi.org/10.5194/essd-10-2141-2018

Los, S. (2013). Analysis of trends in fused AVHRR and MODIS NDVI data for 1982–2006: Indication for a CO_2 fertilization effect in global vegetation. *Global Biogeochemical Cycles*, 27(2), 318–330. https://doi.org/10.1002/gbc.20027

Martens, B., Miralles, D. G., Lievens, H., van der Schalie, R., de Jeu, R. A. M., Fernandez-Prieto, D., & Verhoest, N. E. C. (2017). GLEAM v3: satellite-based land evaporation and root-zone soil moisture. *Geoscientific Model Development*, 10(5), 1903–1925. https://doi.org/10.5194/gmd-10-1903-2017

Mauritsen, T., Bader, J., Becker, T., Behrens, J., Bittner, M., Brokopf, R., & Esch, M. (2019). Developments in the MPI-M Earth System Model version 1.2 (MPI-ESM1. 2) and its response to increasing CO_2. *Journal of Advances in Modeling Earth Systems*, *11*(4), 998–1038. https://doi.org/10.1029/2018MS001400

McCarthy, H. R., Oren, R., Finzi, A. C., & Johnsen, K. H. (2006). Canopy leaf area constrains CO_2-induced enhancement of productivity and partitioning among aboveground carbon pools. *Proceedings of the National Academy of Sciences of the United States of America*, *103*(51), 19356–19361. https://doi.org/10.1073/pnas.0609448103

McColl, K. A., Alemohammad, S. H., Akbar, R., Konings, A. G., Yueh, S., & Entekhabi, D. (2017). The global distribution and dynamics of surface soil moisture. *Nature Geoscience*, *10*(2), 100–104. https://doi.org/10.1038/ngeo2868

Meiyappan, P., Jain, A. K., & House, J. I. (2015). Increased influence of nitrogen limitation on CO_2 emissions from future land use and land use change. *Global Biogeochemical Cycles*, *29*(9), 1524–1548. https://doi.org/10.1002/2015GB005086

Moesinger, L., Dorigo, W., de Jeu, R., van der Schalie, R., Scanlon, T., Teubner, I., & Forkel, M. (2020). The global long-term microwave Vegetation Optical Depth Climate Archive (VODCA). *Earth System Science Data*, *12*(1), 177–196. https://doi.org/10.5194/essd-12-177-2020

Myneni, R., Knyazikhin, Y., & Park, T. (2015). *MOD15A2H MODIS leaf area index/FPAR 8-day L4 global 500m SIN grid V006*. NASA EOSDIS Land Processes DAAC.

Norby, R. J., & Zak, D. R. (2011). Ecological lessons from free-air CO_2 enrichment (FACE) experiments. *Annual Review of Ecology, Evolution, and Systematics*, *42*, 181–203. https://doi.org/10.1146/annurev-ecolsys-102209-144647

Oleson, K., Lawrence, D., Bonan, G., Drewniak, B., Huang, M., Koven, C., Levis, S., Li, F., Riley, W. J., Subin, Z. M., & Yang, Z. (2013). *Technical description of version 4.5 of the Community Land Model (CLM)*. NCAR/TN-503+STR. https://doi.org/10.5065/D6RR1W7M

Piao, S., Sitch, S., Ciais, P., Friedlingstein, P., Peylin, P., Wang, X., & Cong, N. (2013). Evaluation of terrestrial carbon cycle models for their response to climate variability and to CO_2 trends. *Global Change Biology*, *19*(7), 2117–2132. https://doi.org/10.1111/gcb.12187

Poulter, B., Frank, D., Ciais, P., Myneni, R. B., Andela, N., Bi, J., & van der Werf, G. R. (2014). Contribution of semi-arid ecosystems to interannual variability of the global carbon cycle. *Nature*, *509*(7502), 600–603. https://doi.org/10.1038/nature13376

Prentice, I. C., Farquhar, G., Fasham, M., Goulden, M., Heimann, M., Jaramillo, V., Kheshgi, H. S., LeQuéré, C., Scholes, R. J., & Wallace, D. W. (2001). *The carbon cycle and atmospheric carbon dioxide*. Cambridge University Press.

Seneviratne, S. I., Corti, T., Davin, E. L., Hirschi, M., Jaeger, E. B., Lehner, I., Orlowsky, B., & Teuling, A. J. (2010). Investigating soil moisture–climate interactions in a changing climate: A review. *Earth-Science Reviews*, *99*(3), 125–161. https://doi.org/10.1016/j.earscirev.2010.02.004

Sitch, S., Friedlingstein, P., Gruber, N., Jones, S. D., Murray-Tortarolo, G., Ahlström, A., Doney, S. C., Graven, H., Heinze, C., Huntingford, C., Levis, S., Levy, P. E., Lomas, M., Poulter, B., Viovy, N., Zaehle, S., Zeng, N., Arneth, A., Bonan, G., … Myneni, R. (2015). Recent trends and drivers of regional sources and sinks of carbon dioxide. *Biogeosciences*, *12*(3), 653–679. https://doi.org/10.5194/bg-12-653-2015

Smith, B., Warlind, D., Arneth, A., Hickler, T., Leadley, P., Siltberg, J., & Zaehle, S. (2014). Implications of incorporating N cycling and N limitations on primary production in an individual-based dynamic vegetation model. *Biogeosciences*, *11*, 2027–2054. https://doi.org/10.5194/bg-11-2027-2014

Smith, W. K., Fox, A. M., MacBean, N., Moore, D. J., & Parazoo, N. C. (2020). Constraining estimates of terrestrial carbon uptake: New opportunities using long-term satellite observations and data assimilation. *New Phytologist*, *225*(1), 105–112. https://doi.org/10.1111/nph.16055

Smith, W. K., Reed, S. C., Cleveland, C. C., Ballantyne, A. P., Anderegg, W. R. L., Wieder, W. R., Liu, Y. Y., & Running, S. W. (2016). Large

divergence of satellite and Earth system model estimates of global terrestrial CO_2 fertilization. *Nature Climate Change*, *6*(3), 306–310. https://doi.org/10.1038/nclimate2879

Song, X. P., Hansen, M. C., Stehman, S. V., Potapov, P. V., Tyukavina, A., Vermote, E. F., & Townshend, J. R. (2018). Global land change from 1982 to 2016. *Nature*, *560*(7720), 639–643. https://doi.org/10.1038/s41586-018-0411-9

Stevens, N., Lehmann, C. E., Murphy, B. P., & Durigan, G. (2017). Savanna woody encroachment is widespread across three continents. *Global Change Biology*, *23*(1), 235–244. https://doi.org/10.1111/gcb.13409

Tian, F., Brandt, M., Liu, Y. Y., Rasmussen, K., & Fensholt, R. (2017). Mapping gains and losses in woody vegetation across global tropical drylands. *Global Change Biology*, *23*(4), 1748–1760. https://doi.org/10.1111/gcb.13464

Ukkola, A. M., Prentice, I. C., Keenan, T. F., Van Dijk, A. I., Viney, N. R., Myneni, R. B., & Bi, J. (2016). Reduced streamflow in water-stressed climates consistent with CO_2 effects on vegetation. *Nature Climate Change*, *6*(1), 75–78. https://doi.org/10.1038/nclimate2831

Venter, Z. S., Cramer, M. D., & Hawkins, H. J. (2018). Drivers of woody plant encroachment over Africa. *Nature Communications*, *9*(1), 2272. https://doi.org/10.1038/s41467-018-04616-8

Walker, A. P., De Kauwe, M. G., Bastos, A., Belmecheri, S., Georgiou, K., Keeling, R., McMahon, S. M., Medlyn, B. E., Moore, D. J. P., Norby, R. J., Zaehle, S., Anderson-Teixeira, K. J., Battipaglia, G., Brienen, R. J. W., Cabugao, K. G., Cailleret, M., Campbell, E., Canadell, J. G., Ciais, P., … Zuidema, P. A. (2021). Integrating the evidence for a terrestrial carbon sink caused by increasing atmospheric CO_2. *New Phytologist*, *229*(5), 2413–2445. https://doi.org/10.1111/nph.16866

Wittwer, S., & Robb, W. (1964). Carbon dioxide enrichment of greenhouse atmospheres for food crop production. *Economic Botany*, *18*(1), 34–56. https://doi.org/10.1007/BF02904000

Wullschleger, S. D., Tschaplinski, T. J., & Norby, R. J. (2002). Plant water relations at elevated CO_2 – Implications for water-limited environments. *Plant, Cell & Environment*, *25*(2), 319–331. https://doi.org/10.1046/j.1365-3040.2002.00796.x

Xiao, Z. Q., Liang, S. L., Wang, J. D., Chen, P., Yin, X. J., Zhang, L. Q., & Song, J. L. (2014). Use of general regression neural networks for generating the GLASS leaf area index product from time-series MODIS surface reflectance. *IEEE Transactions on Geoscience and Remote Sensing*, *52*(1), 209–223. https://doi.org/10.1109/TGRS.2013.2237780

Zhu, Z., Bi, J., Pan, Y., Ganguly, S., Anav, A., Xu, L., Samanta, A., Piao, S., Nemani, R., & Myneni, R. (2013). Global data sets of Vegetation Leaf Area Index (LAI)3g and Fraction of Photosynthetically Active Radiation (FPAR)3g derived from Global Inventory Modeling and Mapping Studies (GIMMS) Normalized Difference Vegetation Index (NDVI3g) for the period 1981 to 2011. *Remote Sensing*, *5*(2), 927–948. https://doi.org/10.3390/rs5020927

Zhu, Z., Piao, S., Myneni, R. B., Huang, M., Zeng, Z., Canadell, J. G., Ciais, P., Sitch, S., Friedlingstein, P., Arneth, A., Cao, C., Cheng, L., Kato, E., Koven, C., Li, Y., Lian, X. U., Liu, Y., Liu, R., Mao, J., … Zeng, N. (2016). Greening of the Earth and its drivers. *Nature Climate Change*, *6*, 791–795. https://doi.org/10.1038/nclimate3004

SUPPORTING INFORMATION

Additional supporting information may be found online in the Supporting Information section.